Journal of Alloys and Compounds 581 (2013) 653–658

Contents lists available at ScienceDirect

Journal of Alloys and Compounds

journal homepage: www.elsevier.com/locate/jalcom

Low temperature operating $In_{2-x}Ni_xO_3$ sensors with high response and good selectivity for NO_2 gas

Yu Chen [c,1], Linghui Zhu [a,1], Caihui Feng [a], Juan Liu [b], Chao Li [b], Shanpeng Wen [b,*], Shengping Ruan [a,*]

[a] State Key Laboratory on Integrated Optoelectronics, Changchun 130012, PR China
[b] College of Electronic Science and Engineering, Jilin University, Changchun 130012, PR China
[c] Institute of Semiconductors, Chinese Academy of Sciences, Beijing 100083, PR China

ARTICLE INFO

Article history:
Received 21 April 2013
Received in revised form 23 July 2013
Accepted 24 July 2013
Available online 2 August 2013

Keywords:
Stable solid solution
$In_{2-x}Ni_xO_3$
Low temperature
Gas sensing

ABSTRACT

Pure In_2O_3 and solid state solution $In_{2-x}Ni_xO_3$ nanofibers with different Ni-doping concentration were prepared via electrospinning method. Sensor based on $In_{2-x}Ni_xO_3$ nanofibers with 6 (mol)% Ni-doping concentration exhibited the highest response, good selectivity and low detectable concentration limit down to ppb levels of NO_2 at a relatively low temperature of 90 °C. These properties make the $In_{2-x}Ni_xO_3$ nanofibers good candidates for NO_2 detection.

1. Introduction

As the byproduct of fossil fuel combustion, NO_2 is a kind of deadly poison and harmful environmental pollutant [1,2]. NO_2 detection has become a research focus due to the increasing attention on both human health and environmental protection nowadays. During past few decades, metal-oxide semiconductors (MOS) have triggered intense interest in the detection of NO_x gases [1]. Up to date, NO_2 sensors based on MOS such as TiO_2 [2], ZnO [3], SnO_2 [4], In_2O_3 [5], NiO [6], WO_3 [7] and some combinations of them such as ZnO–TiO_2 [8], SnO_2–ZnO [9] have been greatly developed. However, as shown in Table 1, it is somewhat difficult for these previous reported NO_x sensors to achieve low operating temperature (<100 °C) in conjunction with high sensing response at the same time. Hence, more efforts need to be made to achieve higher response and lower operating temperature. Further, low detectable concentration limit (down to ppb level) and good selectivity are also highly recommended in a practical application [1,8].

The gas sensing reaction is reported to be a surface-controlled process for some MOS sensors, and their sensing performance is significantly influenced by both the surface state and morphology of the metal-oxides [1,14,15]. Therefore, one-dimensional (1D) nanofibers (NFs) can deliver favorable performance because of the huge surface-to-volume ratios [16]. What's more, the properties of many MOS gas sensing materials can also be easily tailored by adjusting the rates of impurity elements, and their selectivity and stability are much better than normal metal oxides for gas sensors [17]. For these reasons, the methods of adjusting impurity elements and utilizing 1D structure to prepare NO_2 sensors based on MOS with high performance are of interest.

In the previous studies, In_2O_3 nanostructures have been widely applied for detecting some poisonous [18,19] and VOCs [20,21] due to its low resistance, good catalysis, high sensitivity and strong interaction with gas molecules. Nevertheless, NO_2 sensors based on the In_2O_3-based solid-state solutions with 1D nanostructure, which may show better performances than the pure In_2O_3 based ones, have rarely been concerned. In this paper, the stable solid-state solution $In_{2-x}Ni_xO_3$ NFs were fabricated by doping Ni into In_2O_3 via electrospinning and calcination techniques. Their NO_2-sensing properties were also investigated. Highly efficient sensing performances against low concentration of NO_2 were observed at low temperature, which indicated that the as-synthesized sample is an excellent nanomaterial for detecting NO_2.

2. Experimental

Polyvinylpyrrolidone (PVP, Mw ≈1,300,000) was purchased from Sinopharm Chemical Reagent Co., Ltd., and other chemicals were obtained from Beijing Chemicals Co., Ltd. All the chemicals are of analytical grade and used without further purification. In a typical procedure, 0.4 g $In(NO_3)_3{\cdot}4.5H_2O$ and a suitable amount of $Ni(CH_3COO)_2{\cdot}4H_2O$ were dissolved in the mixture of 4.4 g N,N-dimethylformamide (DMF) and 4.4 g ethanol (EtOH). After the above solution have been stirred for 2 h, 0.8 g PVP was added into it. With further stirring of 6 h, the obtained solution was then loaded into a plastic syringe, which was connected to a high-voltage

* Corresponding authors. Tel./fax: +86 431 85168242.
E-mail addresses: sp_wen@jlu.edu.cn (S. Wen), ruansp@jlu.edu.cn (S. Ruan).
[1] These authors contributed equally to this work.

0925-8388/$ - see front matter © 2013 Elsevier B.V. All rights reserved.
http://dx.doi.org/10.1016/j.jallcom.2013.07.168

Table 1
Brief summary of results reported about NO_2 gas sensors based on MOS materials.

Material	Technique	Optimum operating Tem. (°C)	Response (concentration)	Response/recovery time	Ref.
ZnO thin film	Spin coating method	200	$(R_a-R_g)/R_a \times 100\% = 37.2\%$ (100 ppm)	6.72 s/52.62 s (100 ppm)	[3]
TiO_2 nanoparticles	AC electrophoretic deposition	500	–	1.5 min/2.5 min (2–6 ppm)	[2]
Porous WO_3 film	DC magnetron sputtering	150	$(R_g-R_a)/R_a = 41.2$ (1 ppm)	Recovery time >30 min (<100 °C) (1 ppm)	[10]
In_2O_3 nanoribbons	AC electrophoretic deposition	200	$R_g/R_a = 6$ (2 ppm)	43 min/93 min (2 ppm)	[11]
NiO films	Sol–gel spin coating	200	$(R_a-R_g)/R_a \times 100\% = 23.3\%$ (200 ppm)	20 s/498 s (200 ppm)	[6]
Carbon doped WO_3 nanorods	Radio-frequency magnetron sputtering	250	$R_g/R_a = 348$ (5 ppm)	17 s/50 s (0.1 ppm)	[12]
Graphene–WO_3 nanocomposite	Drop coating technique	250	$R_g/R_a = 133$ (5 ppm)	–	[13]

* R_g and R_a are the electrical resistances in NO_2 gas and air, respectively.

power supply. 25 cm away from the syringe, a piece of plat aluminum foil was placed to collect fibers. When a voltage of 20 kV was provided between the cathode (aluminum foil) and the anode (syringe tip), the electrospun composite NFs were obtained on the foil. Finally, the as-electrospun composite NFs were calcined in air at 600 °C for 4 h to remove organic constituents and convert the precursor into crystal NFs.

The NFs were characterized by X-ray diffractometer (XRD, Shimadzu XRD-6000, Cu Kα radiation); scanning electron microscopy (SEM, XL30 ESEM FEG); transmission electron microscopy (TEM, JEOL JEM-3010); X-ray photoelectron spectrometer (XPS, VG ESCA LAB MKII, Mg Kα radiation); electron spin resonance (ESR, JES-FA 200 ESR spectrometer).

The as-synthesized sample was mixed with deionized water in a weight ratio of 100:25 to form a paste. Then the paste was coated on a ceramic tube with a pair of Au electrodes to form a sensing film. Pt lead wires attaching to these electrodes were used as electrical contacts. The sample was calcined at 300 °C for 2 h, and then a Ni–Cr heating wire was inserted in the tube to be a heater as shown in our previous paper [22].

The gas sensing properties were measured using a static test system. The target vapor was injected into a glass test chamber (about 20 L in volume) and fully mixed with the air. Later, the sensor was put into the test chamber. When the sensitivity reached a constant value, the sensor was taken out to recover in air. The electrical properties of the sensors were measured by a CGS-8 (Chemical gas sensor-8) intelligent gas sensing analysis system (Beijing Elite Tech Co., Ltd., China). The sensor response (S) was measured between 70 °C and 130 °C. We define sensor response as the ratio R_g/R_a, where R_g and R_a are the electrical resistances in NO_2 gas and air, respectively. The time taken by the sensor to achieve 90% of the total resistance change is defined as the response time in the case of adsorption or the recovery time in the case of desorption.

3. Results and discussion

3.1. Material characterization

Fig. 1 shows the XRD patterns of the pure In_2O_3 and $In_{2-x}Ni_xO_3$ NFs with different molar ratios (4 mol%, 6 mol%, and 8 mol%) of Ni.

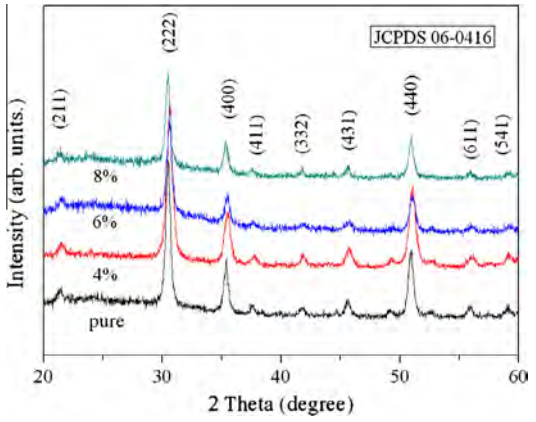

Fig. 1. XRD patterns of the pure In_2O_3 and $In_{2-x}Ni_xO_3$ nanofibers with different Ni-doping concentrations (4 mol%, 6 mol%, and 8 mol%).

It can be seen that all the diffraction peaks correspond to the cubic indium oxide (JCPDS Card No. 06-0416) [23]. For the $In_{2-x}Ni_xO_3$ NFs, no impure phases corresponding to Ni compounds are detected, revealing that the Ni element is effectively inserted into the crystal In_2O_3 lattice and stable $In_{2-x}Ni_xO_3$ substitution solid solution is formed. Moreover, it can be seen that the diffraction peaks of $In_{2-x}Ni_xO_3$ NFs have slightly shifted to the higher angles compared with those of In_2O_3 NFs, which suggests that the particle size of the $In_{2-x}Ni_xO_3$ becomes smaller than that of the pure one [17]. This phenomenon can be explained by Nae-Lih Wu's theory, i.e., because of the interaction on the boundaries between host and dopant crystallites, the motion of crystallites is restricted [14].

To further identify the formation of $In_{2-x}Ni_xO_3$ substitution solid solution and deeply analysis the as-synthesized nanomaterials, XPS and ESR measurements on $In_{2-x}Ni_xO_3$ NFs (6 (mol)% Ni-doping) were carried out. Fig. 2(a) shows the XPS survey spectrum of as-prepared $In_{2-x}Ni_xO_3$ NFs, indicating that the surface of the $In_{2-x}Ni_xO_3$ NFs is composed of In, O, C, and Ni elements. The carbon peak (284.7 eV) is likely to be from the surface contamination. As shown in Fig. 2(b), the double peaks with binding energies at 451.75 eV and 444.15 eV are corresponding to the characteristic spin–orbit split of $In3d_{3/2}$ and $In3d_{5/2}$ signals, respectively [24]. Compared with the reported $In3d_{5/2}$ signal of metallic indium, which appeared at 443.6 eV, there is a chemical shift of 0.5 eV for the $In3d_{5/2}$ peak of the present $In_{2-x}Ni_xO_3$ sample. It indicates that the element indium in $In_{2-x}Ni_xO_3$ NFs exists in the oxide state [25]. The two peaks at Fig. 2(c) with binding energies of 854 eV and 855.6 eV correspond to the Ni^{3+} $2p_{3/2}$ and Ni^{2+} $2p_{3/2}$ respectively. While the ESR spectrum is shown in Fig. 2(d), the signal at $g = 2.30$ is caused by the presence of Ni^{2+} ions in cationic sites of In_2O_3 lattice. The signal at $g = 2.24$ belongs to the Ni^{3+} ions. Whereas the signal at $g = 2.506$ and $g = 1.987$ belong to In^{2+} and In^+, respectively. So the $In_{2-x}Ni_xO_3$ NF is composed of Ni^{2+}, Ni^{3+}, In^+, In^{2+}, In^{3+}, O^{2-}, which reveals the formation of $In_{2-x}Ni_xO_3$ substitution solid solution.

The appearance of Ni^{3+} ions indicates that part of Ni^{2+} ions were transformed into Ni^{3+} with simultaneous formation of In^{2+} ions after high-temperature treatment in air:

$$Ni^{2+} + In^{3+} \Longleftrightarrow Ni^{3+} + In^{2+} \quad (1)$$

The emergence of In^+ is due to an easy electron exchange process in In_2O_3 [26,27]:

$$2In^{2+} \Longleftrightarrow In^{3+} + In^{+} \quad (2)$$

Thus $In_{2-x}Ni_xO_3$ can be expected to have higher In^{2+} concentration than In_2O_3.

Fig. 3 shows the SEM images of the NFs. It can be seen that the composite NFs, which are collected as randomly oriented struc-

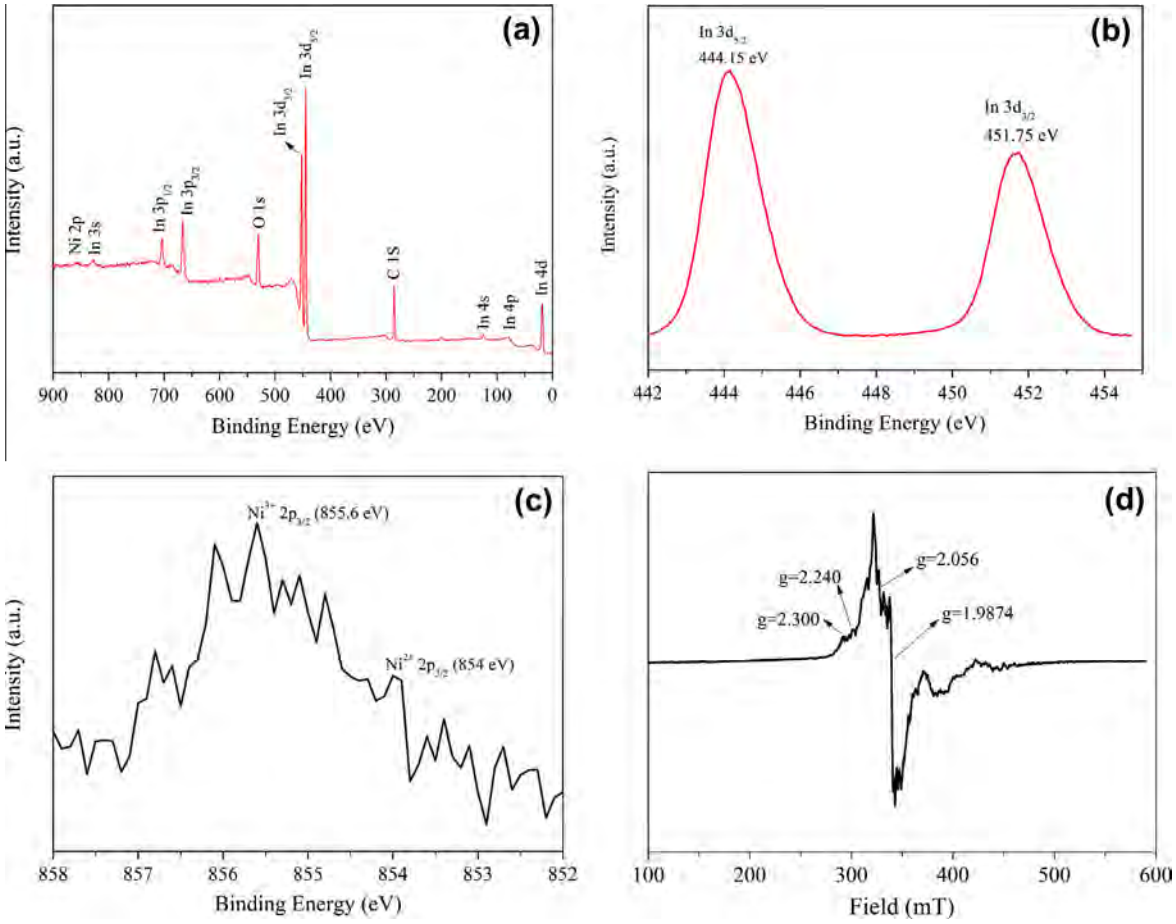

Fig. 2. (a) XPS survey spectrum of as-prepared $In_{2-x}Ni_xO_3$ NFs; (b) XPS peaks of In3d of the $In_{2-x}Ni_xO_3$ NFs; (c) XPS peaks of Ni^{3+} 2p of the $In_{2-x}Ni_xO_3$ NFs; (d) ESR spectrum of the $In_{2-x}Ni_xO_3$ NFs (6 (mol)%).

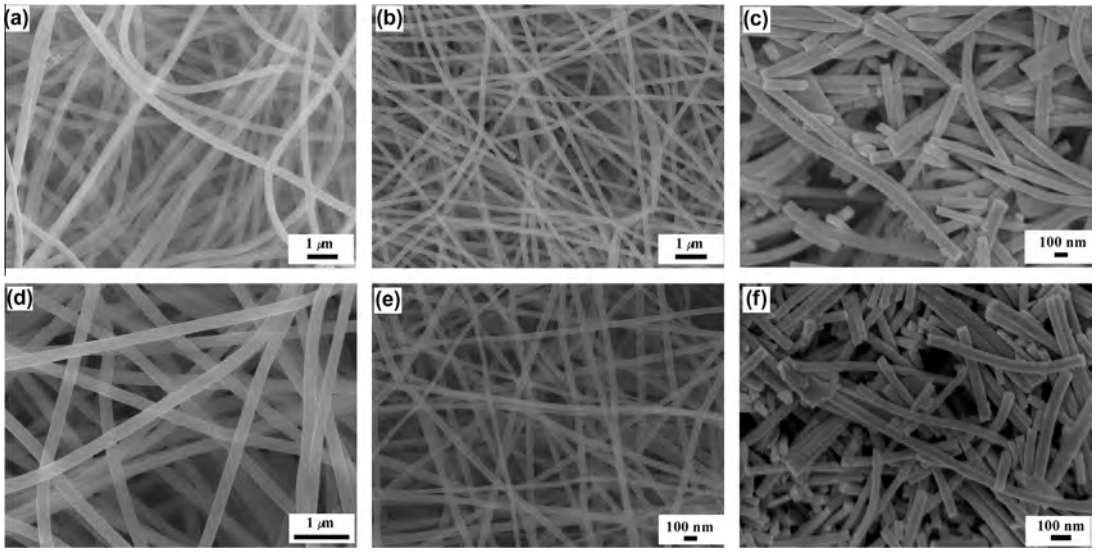

Fig. 3. SEM images of (a) $In(NO_3)_3$/PVP composite nanofibers; (b) In_2O_3 nanofibers; (c) In_2O_3 NFs obtained from the paste after calcinations; (d) $In(NO_3)_3$/ PVP/ $Ni(CH_3COO)_2$ composite nanofibers (6 (mol)% Ni-doping); (e) $In_{2-x}Ni_xO_3$ nanofibers (6 (mol)% Ni-doping); (f) $In_{2-x}Ni_xO_3$ NFs obtained from the paste after calcinations.

tures in the form of nonwoven mats, have smooth and uniform surface. Their average diameters are about 291 nm (In $(NO_3)_3$/PVP) and 409 nm ($In(NO_3)_3$/PVP/$Ni(CH_3COO)_2$) (6 (mol)% Ni-doping), respectively. After calcination at 600 °C, the NFs shrink and become bend and rough, their average diameters were reduced to about 100 nm (In_2O_3) and 62 nm ($In_{2-x}Ni_xO_3$) (6 (mol)% Ni-doping). It is obvious that the average diameter of $In_{2-x}Ni_xO_3$ NFs (62 nm) is smaller than that of the pure NFs (100 nm), which may due to

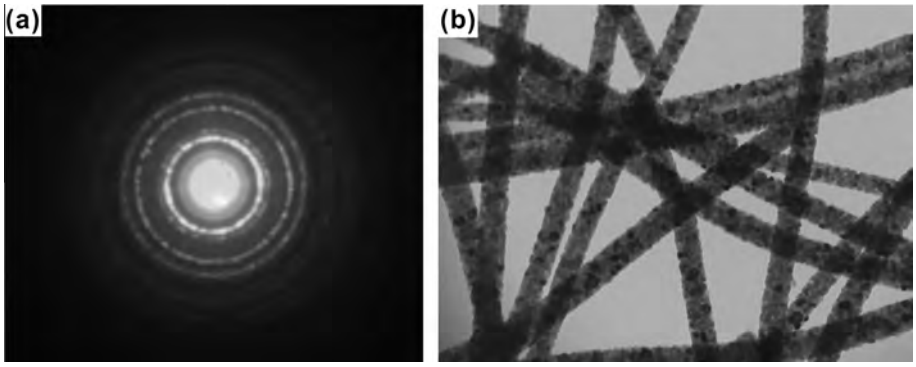

Fig. 4. The (a) SAED pattern and (b) TEM image of $In_{2-x}Ni_xO_3$ nanofibers (6 (mol)% Ni-doping).

the reduced particle size. In_2O_3 and $In_{2-x}Ni_xO_3$ NFs obtained from the paste after calcinations are shown in Fig. 3(c and f), respectively, both of them are broken because of the mixing with deionized water and coating process. Further morphology characterization of $In_{2-x}Ni_xO_3$ NFs (6 (mol)% Ni-doping) were examined by TEM as shown in Fig. 4(a), which agrees with the SEM results. The SAED pattern shown in Fig. 4(b) indicates that $In_{2-x}Ni_xO_3$ NFs are polycrystalline in structure.

The XPS data depicted in Table 2 indicates that atomic percent of lattice oxygen in $In_{2-x}Ni_xO_3$ is less than that in In_2O_3, which means that more oxygen vacancies formed with Ni-doping.

3.2. Gas sensitive properties of the samples

Fig. 5 shows the responses as a function of operating temperature from 70 °C to 130 °C for the pure and $In_{2-x}Ni_xO_3$ NFs (4 (mol)%, 6 (mol)% and 8 (mol)%) exposed to 5 ppm NO_2. In the range of the operating temperatures studied, the response values increase sharply at first and then decrease dramatically. Each curve presents a maximum at same operating temperature of 90 °C. Moreover, the $In_{2-x}Ni_xO_3$ sensor with 6 (mol)% Ni-doping exhibits a higher sensitivity than the other three sensors. For these reasons, 90 °C is believed to be the optimum operating temperature and 6 (mol)% is chosen as the optimum doping concentration.

The response and recovery characteristics of $In_{2-x}Ni_xO_3$ NFs (6 (mol)% Ni-doping) versus different NO_2 concentration at 90 °C are shown in Fig. 6(a). The response values are about 7.2, 12.8, 28.2, 39.7, 107.7 to 0.5, 1, 3, 5, and 10 ppm NO_2, respectively. Furthermore, it can also be seen that the signal from the sensor becomes stable within 580 s after it is exposed to NO_2, and returns to the original values within 650 s after the tested vapor is replaced with air. This relatively long response and recovery times are mainly attributed to the low operating temperature [28]. Fig. 6(b) shows gas response of the sensors versus NO_2 concentrations plots at 90 °C. In the low concentration detecting range (0.5–20 ppm NO_2), the $In_{2-x}Ni_xO_3$ NFs (6 (mol)%) sensor exhibits much higher sensitivity than the pure In_2O_3 one. However, pure In_2O_3 have no response to 0.5 and 1 ppm NO_2, which indicates the $In_{2-x}Ni_xO_3$ NFs with 6 (mol)% Ni-doping has lower detecting limit.

The gas sensing selectivity is another important parameter to evaluate the sensing ability of semiconductor materials. The cross responses of the $In_{2-x}Ni_xO_3$ NFs (6 (mol)% Ni-doping) to 50 ppm

Table 2
XPS data of In_2O_3 and $In_{2-x}Ni_xO_3$ nanofibers.

	Lattice oxygen (at.%)	Absorbed oxygen (at.%)	In (at.%)	Ni (at.%)
In_2O_3	50.29	19.54	30.17	
$In_{2-x}Ni_xO_3$	48.87	20.56	28.5	2.07

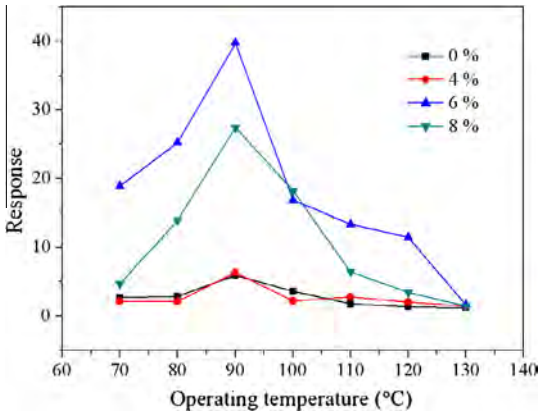

Fig. 5. Responses of pure In_2O_3 NFs and $In_{2-x}Ni_xO_3$ NFs to 5 ppm NO_2 at different operating temperatures.

different gases such as CO, HCHO, CH_4, C_6H_6, H_2S, H_2 and 10 ppm NO_2 at 90 °C are shown in Fig. 7. As shown in this figure, the sensor exhibits much larger response to NO_2 than to other gases. The observed high sensitivity and selectivity of the $In_{2-x}Ni_xO_3$ NFs make the developed $In_{2-x}Ni_xO_3$ NF to be a suitable candidate for monitoring low concentrations of NO_2.

The mechanism of NO_2 detection can be explained as follows. During the gas-sensing measurement, the oxygen molecules in the air (carrier gas) can capture the electrons from the In_2O_3 NFs and form ions (O_2^-, O^- and O^{2-}) adsorbed on the surface of sensing layer, resulting in the formation of a depletion layer at grain boundaries [29]. Upon exposure to NO_2 gas, the NO_2 molecules first contact with and then physically adsorb onto the surface of In_2O_3. NO_2 has higher electron affinity (≈2.28 eV) than that of the pre-adsorbed oxygen (0.43 eV) [30]. So the NO_2 molecules interact with the surface of In_2O_3 through surface-adsorbed oxygen ions, which led to the increase of the resistance and the potential barrier height at grain boundaries, the process of the reaction can be described as follows [31]:

$$NO_{2(gas)} \leftrightarrow NO_{2(ads)} \quad (3)$$

$$e^- + NO_{2(ads)} \leftrightarrow NO_2^-(ads) \quad (4)$$

$$NO_2(gas) + O_2^-(ads) \leftrightarrow NO_2^-(ads) + O_2(gas) \quad (5)$$

The high length-to-diameter ratio, which may help NFs to form netlike structure on the sensor surface, and the large surface-to-volume ratio can make the device absorb a large amount of NO_2 molecules and lead to a high response value in NFs based sensor.

Compared with In_2O_3, $In_{2-x}Ni_xO_3$ NFs show a greater response to NO_2, this can be ascribed to several reasons. Firstly, decreased

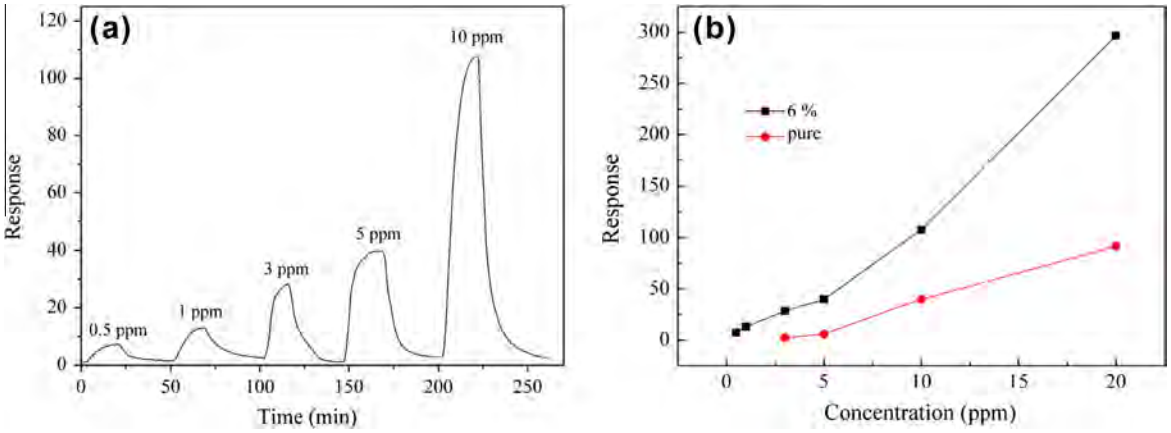

Fig. 6. (a) Response and recovery characteristics of $In_{2-x}Ni_xO_3$ nanofibers (6 (mol)% Ni-doping); (b) responses of the pure In_2O_3 NFs and $In_{2-x}Ni_xO_3$ NFs (6 (mol)% Ni-doping) based sensors versus NO_2 concentrations plots at 90 °C.

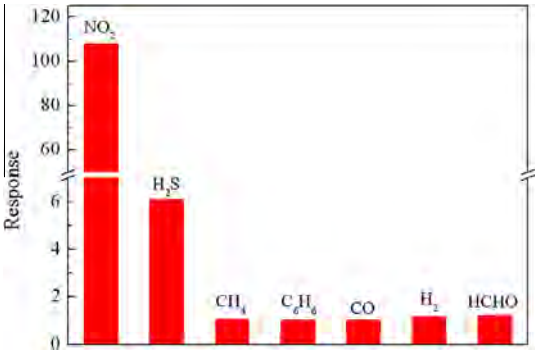

Fig. 7. Responses of $In_{2-x}Ni_xO_3$ nanofibers (6 (mol)% Ni-doping) to different gases at 90 °C.

fiber diameter caused by Ni adding will lead to an increase of NO_2 gas adsorption (shown in Fig. 3), and result in the sensing improvement. Secondly, the formation of $In_{2-x}Ni_xO_3$ can produce more oxygen vacancies, which makes the sensor absorb more NO_2 molecules and improves the sensitivity greatly [32]. Thirdly, at the comparatively low temperatures, NO_2 chemisorption occurs mainly at partially reduced centers (In^{2+}) with the formation of surface complexes: In^{2+}—O—N═O [27]. The higher In^{2+} ions concentration in $In_{2-x}Ni_xO_3$ solid solution structure than that in In_2O_3 can be an important reason for the higher sensitivity to NO_2 of $In_{2-x}Ni_xO_3$ NFs. Lastly, Ni is expected to promote the catalytic process and hence improve gas sensitivity when doped into metal-oxide-semiconductor, which may improve the sensitivity of our $In_{2-x}Ni_xO_3$ sensor further [33].

4. Conclusions

In summary, the pure In_2O_3 and solid state solution $In_{2-x}Ni_xO_3$ NFs with different Ni-doping concentrations were synthesized via electro-spinning method and their NO_2 sensing properties were also investigated. The results show that Ni-doping can reduce the diameters of In_2O_3 NFs and increase the In^{2+} and oxygen vacancy concentrations in $In_{2-x}Ni_xO_3$ solid solution structure, hence improve their NO_2 sensing performance greatly. $In_{2-x}Ni_xO_3$ sensor with 6 (mol)% Ni-doping concentration exhibits the highest response among all samples. The response to 500 ppb NO_2 is 7.2 at a low operating temperature of 90 °C. Moreover, the sensor also exhibits excellent selectivity.

Acknowledgements

The authors are grateful to National Natural Science Foundation of China (Grant Nos. 61275035, 61274068), Chinese National Programs for High Technology Research and Development (Grant No. 2013AA030902), Project of Science and Technology Development Plan of Jilin Province (Grant No. 20120324), and the Opened Fund of the State Key Laboratory on Integrated Optoelectronics (No. IOSKL2012KF03) for the support to the work.

References

[1] M.M. Arafat, B. Dinan, S.A. Akbar, A. Haseeb, Sensors 12 (2012) 7207–7258.
[2] J. Esmaeilzadeh, E. Marzbanrad, C. Zamani, B. Raissi, Sensor. Actuat., B: Chem. 161 (2012) 401–405.
[3] M.A. Chougule, S. Sen, V.B. Patil, Ceram. Int. 38 (2012) 2685–2692.
[4] A. Sharma, M. Tomar, V. Gupta, Sensor. Actuat., B: Chem. 181 (2013) 735–742.
[5] E. Marzbanrad, H. Hassani, B. Raissi, J. Am. Ceram. Soc. (2013) 1–6.
[6] S.R. Nalage, M.A. Chougule, S. Sen, V.B. Patil, J. Mater. Sci.: Mater. Electron. 24 (2013) 368–375.
[7] Y. Qin, F. Wang, W. Shen, M. Hu, J. Alloys Comp. 540 (2012) 21–26.
[8] R. Vyas, S. Sharma, P. Gupta, Y.K. Vijay, A.K. Prasad, A.K. Tyagi, K. Sachdev, S.K. Sharma, J. Alloys Comp. 554 (2012) 59–63.
[9] S. Park, S. An, Y. Mun, C. Lee, ACS Appl. Mater. Interfaces 5 (2013) 4285–4292.
[10] J. Zeng, M. Hu, W. Wang, H. Chen, Y. Qin, Sensor. Actuat., B: Chem. 161 (2012) 447–452.
[11] P. Sowti Khiabani, A. Hosseinmardi, E. Marzbanrad, S. Ghashghaie, C. Zamani, M. Keyanpour-Rad, B. Raissi, Sensor. Actuat., B: Chem. 162 (2012) 102–107.
[12] C. Wongchoosuk, A. Wisitsoraat, D. Phokharatkul, M. Horprathum, A. Tuantranont, T. Kerdcharoen, Sensor. Actuat., B: Chem. 181 (2013) 388–394.
[13] S. Srivastava, K. Jain, V.N. Singh, S. Singh, N. Vijayan, N. Dilawar, G. Gupta, T.D. Senguttuvan, Nanotechnology 23 (2012) 205501.
[14] Y.-F. Sun, S.-B. Liu, F.-L. Meng, J.-Y. Liu, Z. Jin, L.-T. Kong, J.-H. Liu, Sensors 12 (2012) 2610–2631.
[15] J. Huang, X. Xu, C. Gu, S. Yao, Y. Sun, J. Liu, CrystEngComm 14 (2012) 3283–3290.
[16] Z. Wang, Z. Li, J. Sun, H. Zhang, W. Wang, W. Zheng, C. Wang, J. Phys. Chem. C 114 (2010) 6100–6105.
[17] J. Huang, Q. Wan, Sensors 9 (2009) 9903–9924.
[18] N. Singh, R.K. Gupta, P.S. Lee, ACS Appl. Mater. Interfaces 3 (2011) 2246–2252.
[19] M.W.K. Nomani, D. Kersey, J. James, D. Diwan, T. Vogt, R.A. Webb, G. Koley, Sensor. Actuat., B: Chem. 160 (2011) 251–259.
[20] Z. Li, Y. Dzenis, Talanta 85 (2011) 82–85.
[21] J. Liu, T. Luo, F. Meng, K. Qian, Y. Wan, J. Liu, J. Phys. Chem. C 114 (2010) 4887–4894.
[22] C. Feng, S. Ruan, J. Li, B. Zou, J. Luo, W. Chen, W. Dong, F. Wu, Sensor. Actuat., B: Chem. 155 (2011) 232–238.
[23] T. Gao, T. Wang, J. Cryst. Growth 290 (2006) 660–664.
[24] C. Chen, D. Chen, X. Jiao, S. Chen, J. Phys. Chem. C 111 (2007) 18039–18043.
[25] B. Pujilaksono, U. Klement, L. Nyborg, U. Jelvestam, S. Hill, D. Burgard, Mater. Charact. 54 (2005) 1–7.
[26] M. Ivanovskaya, P. Bogdanov, Sensor. Actuat., B: Chem. 53 (1998) 44–53.
[27] P. Bogdanov, M. Ivanovskaya, E. Comini, G. Faglia, G. Sberveglieri, Sensor. Actuat., B: Chem. 57 (1999) 153–158.
[28] L. You, Y.F. Sun, J. Ma, Y. Guan, J.M. Sun, Y. Du, G.Y. Lu, Sensor. Actuat., B: Chem. 157 (2011) 401–407.

[29] J. Xu, J. Han, Y. Zhang, Y.a. Sun, B. Xie, Sensor. Actuat., B: Chem. 132 (2008) 334–339.
[30] N.D. Hoa, S.A. El-Safty, Chem. – Eur. J. 17 (2011) 12896–12901.
[31] K. Wetchakun, T. Samerjai, N. Tamaekong, C. Liewhiran, C. Siriwong, V. Kruefu, A. Wisitsoraat, A. Tuantranont, S. Phanichphant, Sensor. Actuat., B: Chem. 160 (2011) 580–591.
[32] L. Liu, S. Li, J. Zhuang, L. Wang, J. Zhang, H. Li, Z. Liu, Y. Han, X. Jiang, P. Zhang, Sensor. Actuat., B: Chem. 155 (2011) 782–788.
[33] Y. Zheng, J. Wang, P. Yao, Sensor. Actuat., B: Chem. 156 (2011) 723–730.